water

MDPI

Article

Experimental and Numerical Study on Flow Control Using 3-Array Submerged Vane in Laboratory Channel Bend

Bestami Taşar [1], Fatih Üneş [1], Ercan Gemici [2] and Martina Zelenakova [3,*]

[1] Department of Civil Engineering, Iskenderun Technical University, İskenderun 31200, Turkey
[2] Department of Civil Engineering, Bartın University, Bartın 74100, Turkey
[3] Department of Environmental Engineering, Technical University of Kosice, 042 00 Kosice, Slovakia
* Correspondence: martina.zelenakova@tuke.sk

Abstract: Regulation structures such as submerged vane are needed to reduce and eliminate environmental damage due to increased flooding in rivers. In particular, scours on the outer bank due to increased flow velocities cause the river bed to change and deteriorate. In this study, the effect on flow velocities was investigated experimentally by using 3-array submerged vane structures in areas close to the outer bank. The experimental vane results were performed in the open channel setup. The Computational Fluid Dynamics (CFD) results obtained with the numerical model were also verified and compared with experimental results. It has been observed that the CFD model gives results close to the real experimental results. The standard-based k-ε model was used as the turbulence model. In the outer meander, the 3-array submerged vane with a 3-vane structure was found to affect the flow velocity by 16–27% in the region behind the vane. The flow velocities were investigated along with depth using the CFD and found that the mean velocity was reduced by 14–21% along the depth. It is also recommended that submerged vane structures can be applied as an effective method in reducing flow velocities and directing flows.

Keywords: submerged vane; meander; experiment; computational fluid dynamics; open channel flow

Citation: Taşar, B.; Üneş, F.; Gemici, E.; Zelenakova, M. Experimental and Numerical Study on Flow Control Using 3-Array Submerged Vane in Laboratory Channel Bend. *Water* **2023**, *15*, 659. https://doi.org/10.3390/w15040659

Academic Editor: Giuseppe Pezzinga

Received: 28 December 2022
Revised: 28 January 2023
Accepted: 29 January 2023
Published: 8 February 2023

1. Introduction

Regarding, river meandering regulation and especially submerged vane studies, the complexity of the subject matter is unsteady and nonlinear due to the effect of more parameters on the event, and has been studied by very few researchers in the past. Therefore, there is very limited laboratory study. Studies conducted with a submerged vane in meander curves in the 1980s by Odgaard and Kennedy, Odgaard and Lee, Odgaard [1–4] pioneered the entry of submerged vane into the literature as a new method. Marelius and Sinha [5] conducted a study to create the optimum vane angle required to create the strongest secondary circulation in the open channel flow. Voisin and Townsend [6] investigated the optimal size of submerged vanes to protect meandering riverbanks. Gemici [7] investigated the effects of different Froude numbers, vane arrangement, vane length/vane height and approach angle combinations on flow velocity. Mohammediun et al. [8] conducted their research to reduce sedimentation and erosion potential at the junction of curved and straight channels. Fathi et al. [9] investigated the effects of submerged vanes on scrubbing around a vertical wall and overflow abutments with laboratory results. Kalathil et al. [10] used submerged vanes to control sediment entry into the inlet channel with a physical model. Zarei et al. [11] investigated the effects of submerged vanes around the bridge pier and on bed topography changes. Lake et al. [12] investigated the effect of river-based, submerged vane structures in Australia. Gumgum and Cardoso [13] investigated the effects of different vane parameters and water discharge ratios on the bed morphology around a 90° lateral water diversion. Bor [14] studied a 90° water intake to study 3D flow patterns and sediment distribution using submerged vanes. 3D velocity components were measured

using acoustic Doppler velocimetry (ADV). According to her study, downstream corner of the intake, high velocities were measured where scouring occurred.

In this study, the vane experiments were further validated by the numerical method. As a numerical approach, Computational Fluid Dynamics (CFD) was applied to the open channel flow conditions. Ansys-Fluent program containing CFD rules was used. CFD is a branch of fluid mechanics in which problems affecting fluid behavior are analyzed by solving them in 3 dimensions with numerical methods and algorithms. In complex geometries, viscosity, flow velocity, temperature differences etc. the solution is very difficult, if not often impossible, when the parameters are applied to the fundamental equations of fluid mechanics. In CFD methods, the three basic equations governing the fluid motion, continuity, momentum and energy equations are taken as a basis. These equations are solved numerically to reach the pressure, velocity etc. of the flow variables depending on these parameters [15–18]. The flow domain is divided into finite volumes in which discretized versions of the equations governing the flow are written.

When the past studies were examined, it has been determined that there were very few or limited studies to reduce/prevent scours caused by high flow velocities in the meandering of the rivers. This study focuses on the effect of the submerged vane, which is accepted as a new method [19], on the meandering open channel. In this study, experiments at the open channel laboratory were performed on the bend part with 3-array 9 submerged vane and without submerged vane. CFD models are verified by Open channel experiments without vane and 3-array with 9 submerged vanes situations. The submerged vane experiments conducted in this study will contribute to the subject by researching the originality of the river meanders and the effect of the vane. In addition, flow velocities in the open channel were modeled with the CFD method and the cross-sectional flow velocity changes were investigated along the depth.

2. Materials and Methods

The performance of without vane and 3-array with 9 submerged vanes models in meandering open channel flows has been investigated by using a flow discharge of 25 L/s in this study. Detailed information about the experimental setup, experimental conditions and mathematical model for the without-vane and with-vane experiments conducted in the open channel are given below.

2.1. Experimental Set-Up

In Bartın University Hydro-mechanic Laboratory, a 30 cm wide curvilinear channel was built within a 50 cm wide rectangular channel within the existing open channel system. Flow condition details for the experiment are given in Table 1. Q, B, d, A, T, Rh, Fr and V_{mean} denote the discharge flow, channel width, depth of flow, wetted area, wetted perimeter, hydraulic radius, flow Froude number and inlet mean flow velocity in Table 1. In this study, since the Froude number is less than 1, it was observed that there is a subcritical flow or river regime.

Table 1. The Flow conditions for the submerged vane experiment.

Q (m^3 s^{-1})	B (m)	d (m)	A (m^2)	T (m)	R_h (m)	V_{mean} (m s^{-1}) (m s^{-1})	Fr
0.025	0.300	0.095	0.0285	0.490	0.058	0.900	0.94

In order for the flow to occur in river conditions, the bottom of the channel was laid with 15 cm of sediment (gravel) material and the base of the vane was placed on the sand of 5 cm. The experimental conditions prepared for the "with vanes" situation was also provided for the without vane situation. With the start of the pump, the water drawn from the main reservoir passes through the gravel filters and reaches the rectangular channel. With the ultrasonic flow meter, the flow discharge given to the channel through the pipe

was determined. For the desired test set, the flow discharge is fixed by adjusting the vane. It was waited for 10–15 min for the flow conditions to stabilize. Flow discharge adjustments were made with an ultrasonic flow meter (Figure 1c). When the measurements were completed, the base of the channel was corrected, and a new setup was created for the other set. Details of 9 submerged vane experiments with 3 arrays were given in Figure 1a.

Figure 1. Experimental details for submerged vane (**a**) "with vane" situation (**b**) ADV device for velocity determination (**c**) Flowmeter for channel flow.

The flow discharges were measured by an Acoustic Doppler Velocimetry (ADV) flowmeter (Figure 1b). Measurements were made at 60% (0.6 d) of the depth. The working principle of the velocity meter is that the 2 acoustic receivers at the end determine the flow velocity by sending a signal.

In order to reduce the turbulence of the flow entering the channel, the energy of the water was reduced by taking the water entering with the pump into the settling tank. The open channel assembly in which the submerged vane experiment was performed had a base slope of 0.0003. A meandering channel, approximately 3 m long and 30 cm wide, was constructed along the 50 × 50 sectioned rectangular channel. A curved 30° channel bend connects to the upstream and downstream channels. The center radius of the curvature is R = 3.60 m. The vane is made of sheet metal with a thickness of 2 mm. On the bottom of the submerged vane, a 5 mm thick sheet of material was mounted in accordance with the slope/dimensions of the meandering channel and was removed and installed during each experiment. These dimensions have also been considered in the numerical simulations. The experimental setup and sectional information were shown in Figure 2.

The submerged vane experimental setup is given in the above Figure 3. for the "with vane" case. The design for submerged vane experiments, 3D flow velocity modeling and analysis of the experimental results will be emphasized. The presented submerged vane and previously experimental details were given in Table 2.

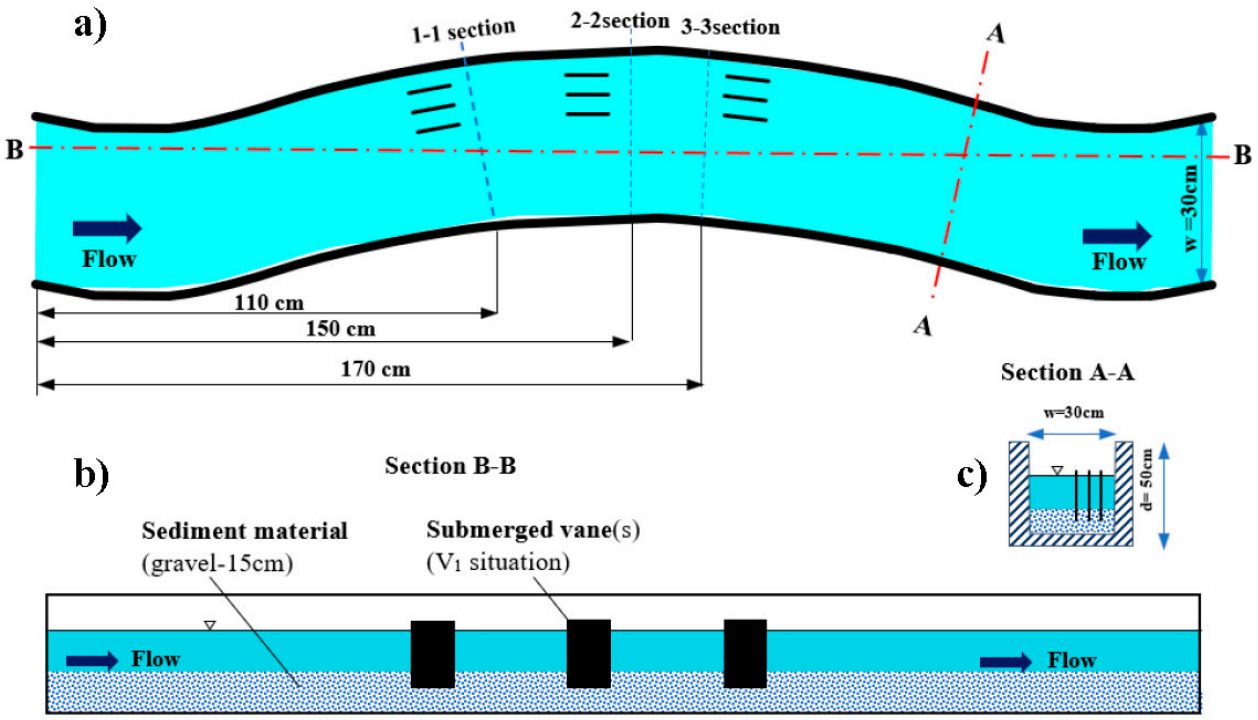

Figure 2. Submerged vane experimental set-up for "with vane" situation: (**a**) Channel top (plan) view, (**b**) Cross section view, (**c**) Section view.

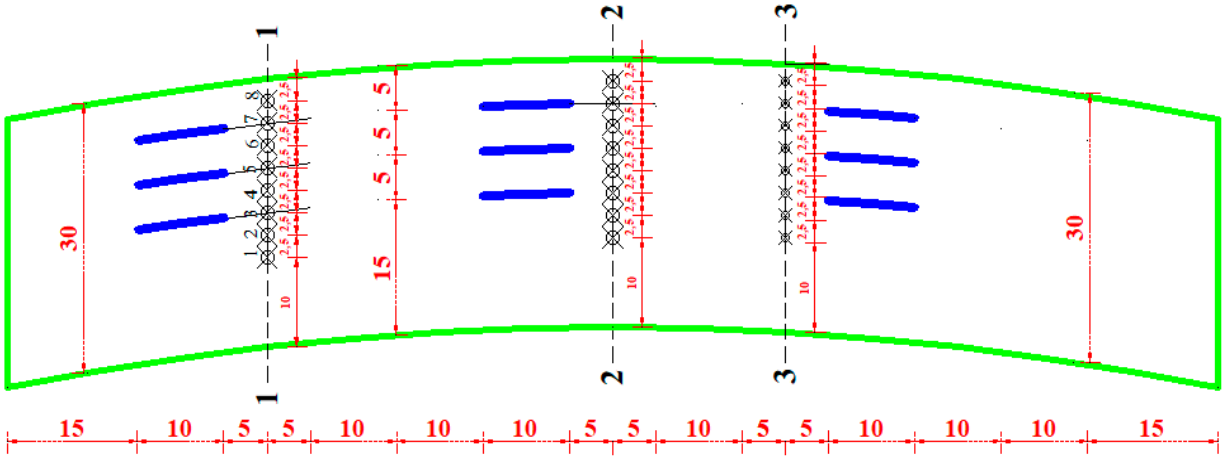

Figure 3. According to "with vane" situation, all sections and points measured in the channel.

Table 2. Presented submerged vane and previously experimental details.

	Presented Study	Odgaard [19]
Vane height/length (cm)	10/10	7.4/15.2
Meander angle (°)	30	90
Bend radius (m)	3.60	11.89
Flow discharge (m^3/s)	0.025	0.11–0.15
Mean velocity (m/s)	0.900	0.396
Water surface slope	0.0003	0.00064
Mean flow depth (cm)	11 (V_0 case), 12 (V_1 case)	17.4 and 18.2

2.2. Mathematical Model

The flow conditions of modeling are turbulent flow and free surface flow which is directed by gravity. According to the literature, this kind of free surface flow can be simulated

by the volume of fluid (VOF) method as water-air 2-phase flow problems. The standard *k*-ε turbulence model was used in the three-dimensional numerical simulation of flow. The *k*-ε turbulence model was a possible method for the free surface flow simulations [20,21].

2.2.1. Basic Equations

The investigated open channel flow was a 3D, turbulent, unsteady free surface flow. For the *k*-ε turbulence model given by [22], the continuity equation, the momentum equation, and the equations for *k*-ε were given Equations (1)–(6).

Continuity equation:

$$\frac{\partial \rho}{\partial t} + \frac{\partial \rho u_i}{\partial x_i} = 0 \tag{1}$$

Momentum equation:

$$\frac{\partial \rho u_i}{\partial t} + \frac{\partial}{\partial x_j}(\rho u_i u_j) = -\frac{\partial P}{\partial x_i} + \rho g + \frac{\partial}{\partial x_j}\left[(\mu + \mu_t)\left(\frac{\partial u_i}{\partial x_j} + \frac{\partial u_j}{\partial x_i}\right)\right] \tag{2}$$

Turbulence kinetic energy (*k*) equation:

$$\frac{\partial(\rho k)}{\partial t} + \frac{\partial(\rho k u_i)}{\partial x_i} = \frac{\partial}{\partial x_i}\left[\left(\mu + \frac{\mu_t}{\sigma_k}\right)\frac{\partial k}{\partial x_i}\right] + G - \rho\varepsilon \tag{3}$$

Turbulence dissipation rate energy (ε) equation:

$$\frac{\partial(\rho\varepsilon)}{\partial t} + \frac{\partial(\rho u_i \varepsilon)}{\partial x_i} = \frac{\partial}{\partial x_i}\left[\left(\mu + \frac{\mu_t}{\sigma_\varepsilon}\right)\frac{\partial \varepsilon}{\partial x_i}\right] + C_{1\varepsilon}\frac{\varepsilon}{k}G - C_{2\varepsilon}\rho\frac{\varepsilon^2}{k} \tag{4}$$

where, t is the time; u_i is the velocity components; x_i is the coordinate components; ρ is the density; g is the gravity; μ is the molecular viscosity; P is the correct pressure; μ_t is the turbulent viscosity, which can be derived from the turbulent kinetic energy k and turbulent dissipation rates:

$$\mu_t = \rho C_\mu \frac{k^2}{\varepsilon} \tag{5}$$

$$G = \mu_t\left(\frac{\partial \mu_i}{\partial x_j} + \frac{\partial u_j}{\partial x_i}\right)\frac{\partial u_i}{\partial x_j} \tag{6}$$

σ_k and σ_ε are turbulence Prandtl numbers for k and ε equation, respectively, σ_k = 1.0, σ_ε = 1.3, $C_{1\varepsilon}$ and $C_{2\varepsilon}$ are ε equation constants, $C_{1\varepsilon}$ = 1.44, $C_{2\varepsilon}$ = 1.92. C_μ = 0.09 is a constant, determined by experimentally.

VOF model

In this study, the VOF method was used to calculate the water-air interface. This method was used for 2-phase air-water flow simulation [23] and to compute the free surface of the flow [24]. The VOF method essentially determines whether the element volumes in the computational mesh are empty, partially filled, or completely filled with water. Representing the volumetric filling ratio of the mesh elements, the mesh element is fully filled for F = 1, empty (filled with air) for F = 0, and partially filled with water for 0 < F < 1 [25]. In this approach, the tracking interface between air and water is accomplished by the solution of a continuity equation for the volume fraction of water:

$$\frac{\partial \alpha_w}{\partial t} + \frac{\partial \alpha_w u_i}{\partial x_i} = 0 \tag{7}$$

where, α_w is volume fraction of water. In each cell, the sum of the volume fractions of air and water is unity. Volume fractions of air denote αa can be given as,

$$\alpha_w + \alpha_a = 1; \qquad 0 \le \alpha_w \le 1 \tag{8}$$

In open channel flows, Ansys-Fluent internally calculates the volume fraction based on the input parameters specified in the boundary conditions. For subcritical inlet flows (Fr < 1), Ansys-Fluent reconstructs the volume fraction values on the boundary by using the values from the neighboring cells. For subcritical inlet flows, node values of volume fraction at the boundary must calculate using the cell values and volume fraction at each face of the boundary must calculate using the interpolated node values. For supercritical inlet flows (Fr > 1), the volume fraction value on the boundary can be calculated using the fixed height of the free surface from the bottom [26].

2.2.2. Boundary Conditions for Submerged Vanes

Flow field boundary conditions must be specified differently on walls, channel inlet, outlet and free surface, due to unsteady and channel flow. Since the boundary and initial conditions are different for each variable, they must be selected separately. Velocities on free surfaces and at side-bottom channels, velocities on submerged vane faces were obtained using the standard wall function based on the recommendation of Launder and Spalding [22]. This wall function accepts a log-law velocity profile close to the wall and was determined as in Equation (9):

$$\frac{u_p}{u_*} = \frac{1}{K} ln\left(E\frac{u_* y_p}{v}\right) \tag{9}$$

where, "up" is the average stream flow velocity at the "p" point; "K" von Karman constant (0.418); "y_p" is the distance from point p to the wall; empirical constant "E" has the value of 9.79; "u_*" is the friction velocity. The "u" uniform velocity distribution was given to the horizontal velocity component in the x-direction at the inflow boundary. The vertical velocity component "v" in the y-direction was set to zero. The inlet velocity field to the channel consists of a forward 'u' horizontal velocity and zero 'v' vertical velocities at all points except points close to the channel.

The wall y^+ is a dimensionless distance similar to the local Reynolds number often used in CFD to indicate how the mesh is for a particular flow. It determines whether the effects in cells adjacent to the wall are laminar or turbulent [27].

$$y^+ = \frac{u_\tau y}{\nu} \tag{10}$$

$$u_\tau = \sqrt{\frac{\tau_w}{\rho}} \tag{11}$$

where u_τ is the friction velocity, y is the height from the wall to the mid-point of the wall-adjacent cells, v is the kinematic viscosity, τ_w is the wall shear stress and ρ is the fluid density at the wall. Values of y^+ close to the lower bound ($y^+ \approx 30$) are most desirable for wall functions, whereas values of $y^+ \approx 1$ are better for near-wall modelling [28].

2.2.3. Meshing-Grid Information

In this paper, the 3D analysis was built up for V_0 and V_1 cases. CFD model was created according to the open channel experiment (Figures 1 and 2). Initial and boundary conditions were established according to the experimental study. 1,927,650 meshes for V_0 submerged vane case and for the V_1 case, 1,938,869 meshes were assigned. In addition, tetrahedron-type meshes were used in the design.

The proposed model was used to simulate the variation of submerged vane open channel flow. The biggest problem during the implementation of the submerged vane in the Fluent model was the skewness error of the network grid. The mesh qualities were controlled with equiangular skewness, equisize skewness and aspect ratio in the Gambit program. Skewness and other problems were solved by acquiring a smaller mesh dimension grid line. Since the real shape of the vane was considered in the model, the skewness error was increased due to the shape of the open channel. Those errors were

defined and corrected by increasing the amount of mesh with Gambit. However, when the mesh becomes smaller, the number of mesh was increased. Furthermore, the computational domains for all cases were approximately divided by 1,927,650–1,938,869 tetrahedral mesh volumes to obtain acceptable skewness coefficients. This represents approximately 315,000 nodes. In the meshing cases, the convergence criterion of flow parameters was taken at 0.01 for all runs.

The 3D analysis was built up for V_0 and V_1 cases. The CFD model was created according to the open channel experiment setup consisting of 1 main meander channel (Figures 1 and 2). According to the experimental inlet measure (Table 1), inlet conditions and boundary layer conditions were established. The boundary conditions of the flow formed with V_0 and V_1 cases have been defined. Figure 4 shows the surfaces for the CFD model solution. According to Figure 4, the water inlet height = velocity inlet, submerged vane − open channel surfaces = wall and outlet section (in downstream) = outflow were accepted. In addition, for the flow discharge of 25 L/s, the water inlet height was defined as 9.5 cm.

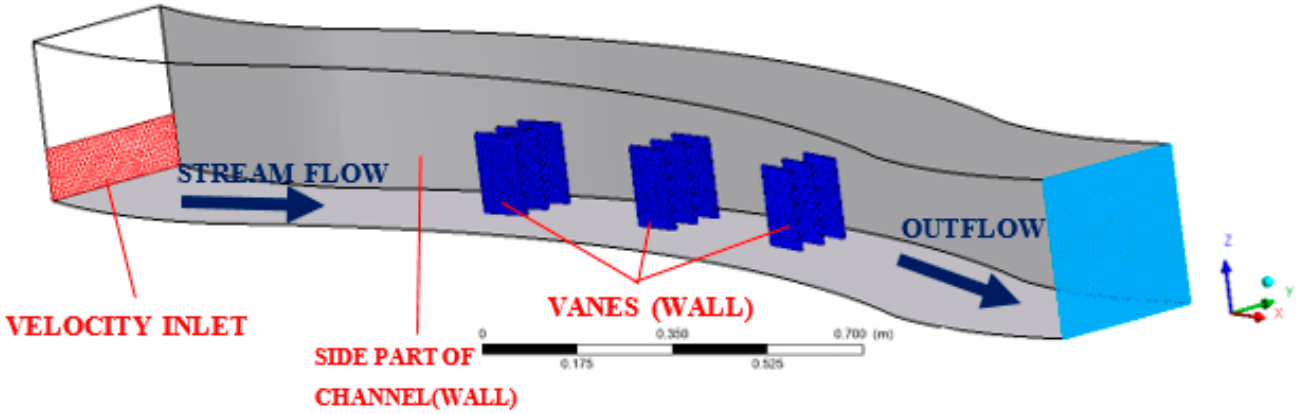

Figure 4. Boundary conditions for "with vanes" situation according to the downstream view.

The mesh independence test was performed by doubling the mesh numbers in the lateral and vertical directions. However, no significant difference in flow velocity results was observed due to mesh improvement. This finding showed that the flow velocity results were independent of the mesh.

2.2.4. Numerical Solver

When the velocity fields in the open channel have complex currents such as circulation flow, turbulent flow and secondary flow problems arise because the open channel flows are nonlinear and velocity–the pressure field interdependent. These problems were solved using the "Coupled" procedure approach. This procedure was the iteration method, and it was based on the prediction-corrector approach. Fluent provides the option to choose "Coupled" pressure-velocity coupling algorithms. The full implicit scheme was used in the model [29]. As an initial state, the inlet channel is first filled with air and water. Next, water at a certain height was released into the free flow at a certain rate from the inlet channel to the upstream end. The channel flow continues until it reaches the downstream limit. The calculation continued for about 600 s, at which point the front had already crossed the downstream boundary and any change in flow area was ignored. A time step of 1 s was chosen after preliminary trials to have the desired converged solution. The discretization methods and solver settings are presented in Table 3.

Table 3. Numerical model details.

Solver Set	**Solver Space-Time**	**Pressure Based 3D, Unsteady**
Model	Multiphase Model Viscous Model	VOF *k-ε*
Phase	Primary Phase Secondary Phase	Air water
Discretization	Pressure Momentum	Presto Second order upwind
Pressure-Velocity Coupling	Method	Coupled
Convergence Criterion	Residuals	0.001 (Continuity) 0.001 (Momentum)

3. Results and Discussion

Flow velocity simulations at the measurement points of the Open Channel were investigated experimental and CFD results. In addition, the numerical results of submerged vane structures were examined along the depth for vane and no vane cases flow velocities. In order to see the amount of change after the section, the measured and simulated flow velocity results are dimensionless based on the average velocity (in Table results). Velocity vectoral representation at 0.6 d for without vane and with vane models given in Figure 5a,b.

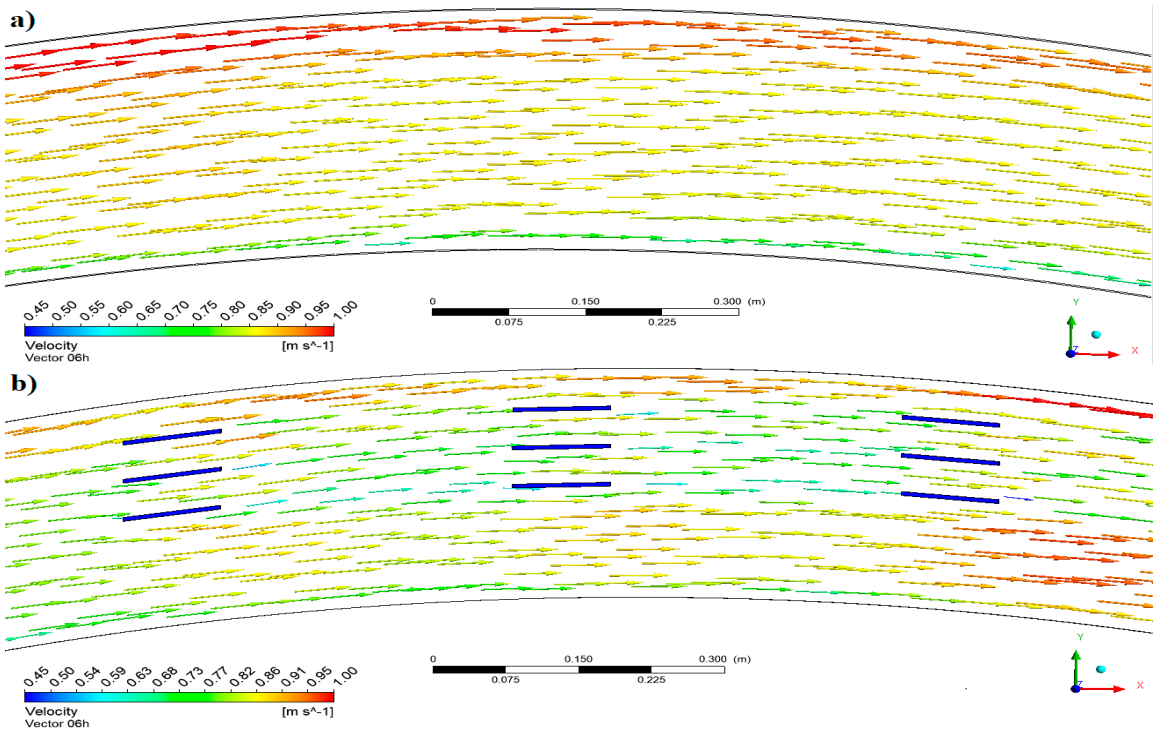

Figure 5. Velocity vectoral representation at 0.6 h for: (**a**) "without vane" situation, (**b**) "with vanes" situation.

When Figure 5a,b were examined, it was observed that high flow velocities are observed at the points where the channel bending first starts. The flow velocity increases (from green to "yellow-orange-red") from the inner bank to the outer bank. When Figure 5b were considered, it was observed that the flow velocity around the vane was reduced (in green color) and between the vanes (yellow color) it had a flow velocity of 0.65–0.75 m/s. It has been seen that flow has a velocity of 0.85–0.93 m/s, near the middle outer bank region and in channel parts without vane (Figure 5a). In order to see the changes in the water

surface, it is given as a velocity contour map in Figure 6 with "without vane" and "with vanes". As can be seen from the figures, it is observed that the flow is directed around the vane and the flow velocity between the vanes decreases. It is seen that the vane structures are effective in directing the flow and reduce the flow velocity, and the flow reaches balance in the inner bank and outer bank in the section of the channel bend. In Table 4, Figures 7 and 8, CFD results are given with the measured points according to the 1-1, 2-2 and 3-3 sections.

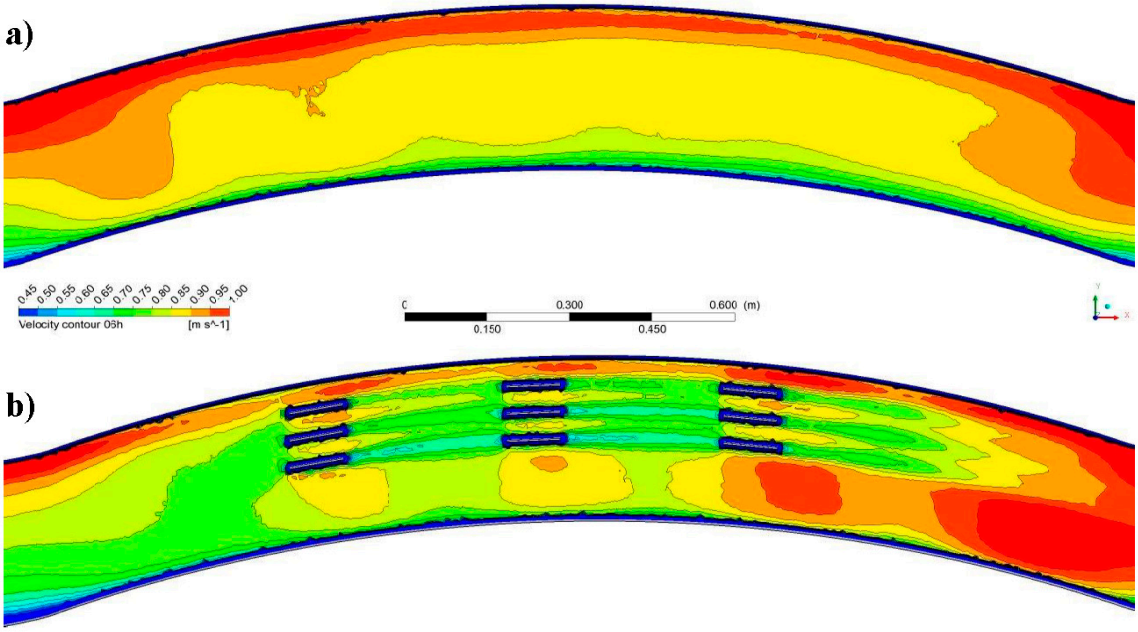

Figure 6. Velocity contour map at the water surface for: (**a**) without vane situation, (**b**) with vanes situation.

Table 4. CFD and experimental velocity results for without vane situation at Section 1-1, 2-2, 3-3.

Section No	Point No	Location at x Direction (m)	Location at y Direction (m)	Experiment Results	Fluent CFD Results	Error (%)
1-1	1	1.10	0.247	0.96	0.97	0.97
	2	1.10	0.272	0.98	0.97	1.08
	3	1.10	0.297	0.98	0.97	0.74
	4	1.10	0.322	0.98	0.97	0.67
	5	1.10	0.347	1.02	0.97	4.77
	6	1.10	0.372	1.02	0.99	2.53
	7	1.10	0.397	1.02	1.04	2.78
	8	1.10	0.422	1.04	1.10	5.89
2-2	1	1.50	0.247	0.98	0.97	1.11
	2	1.50	0.272	0.98	0.98	0.21
	3	1.50	0.297	0.97	0.97	0.08
	4	1.50	0.322	0.97	0.97	0.44
	5	1.50	0.347	1.01	0.97	3.68
	6	1.50	0.372	1.01	0.99	2.36
	7	1.50	0.397	1.03	1.05	1.45
	8	1.50	0.422	1.04	1.10	5.17
3-3	1	1.70	0.247	0.96	0.96	0.90
	2	1.70	0.272	0.97	0.97	0.42
	3	1.70	0.297	0.98	0.97	0.67
	4	1.70	0.322	0.99	0.97	1.44
	5	1.70	0.347	1.00	0.99	1.40
	6	1.70	0.372	1.02	1.01	0.72
	7	1.70	0.397	1.04	1.06	2.21
	8	1.70	0.422	1.06	1.07	0.60

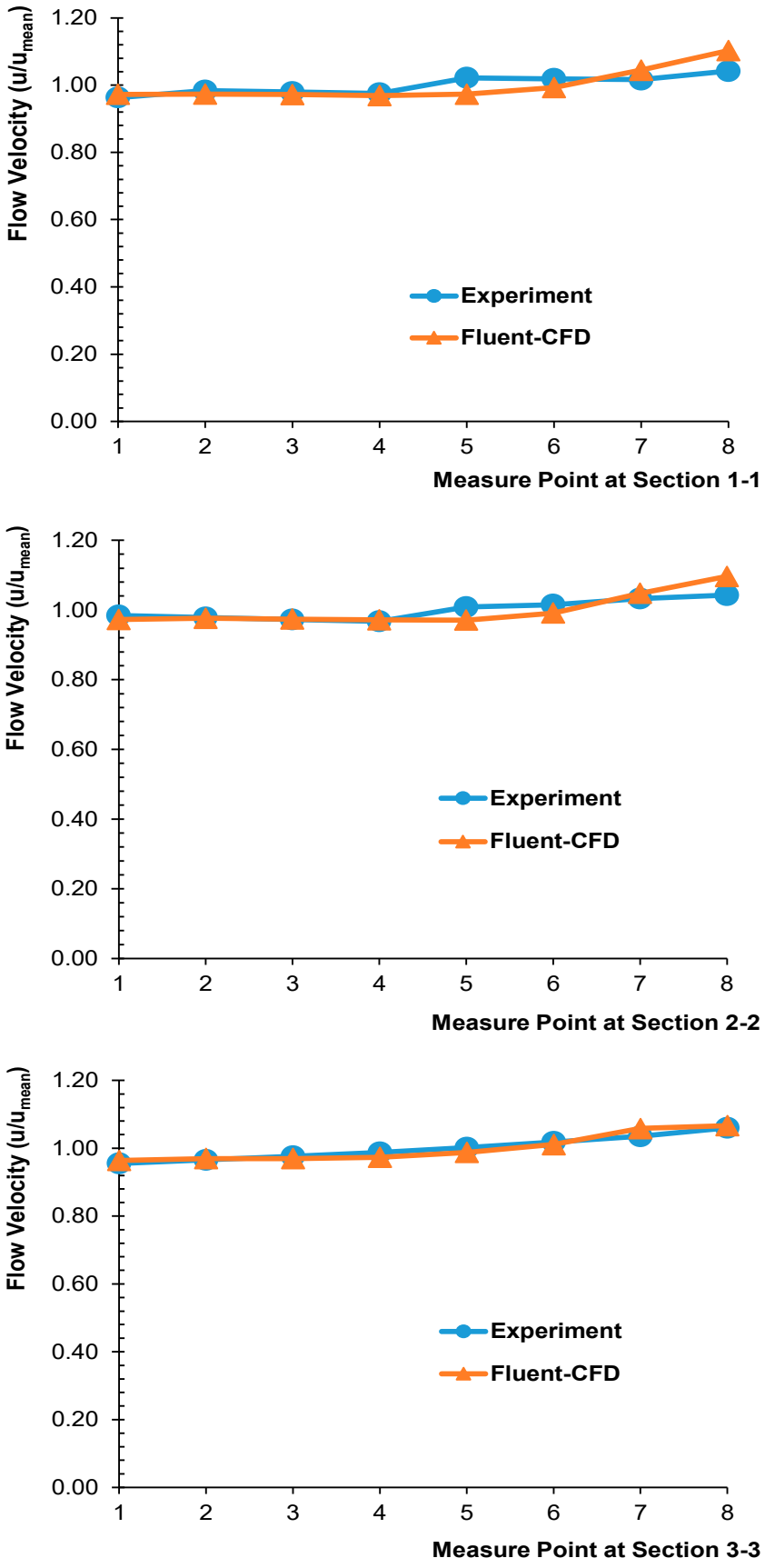

Figure 7. Flow velocity variation for without vane situation at Sections; 1-1, 2-2 and 3-3.

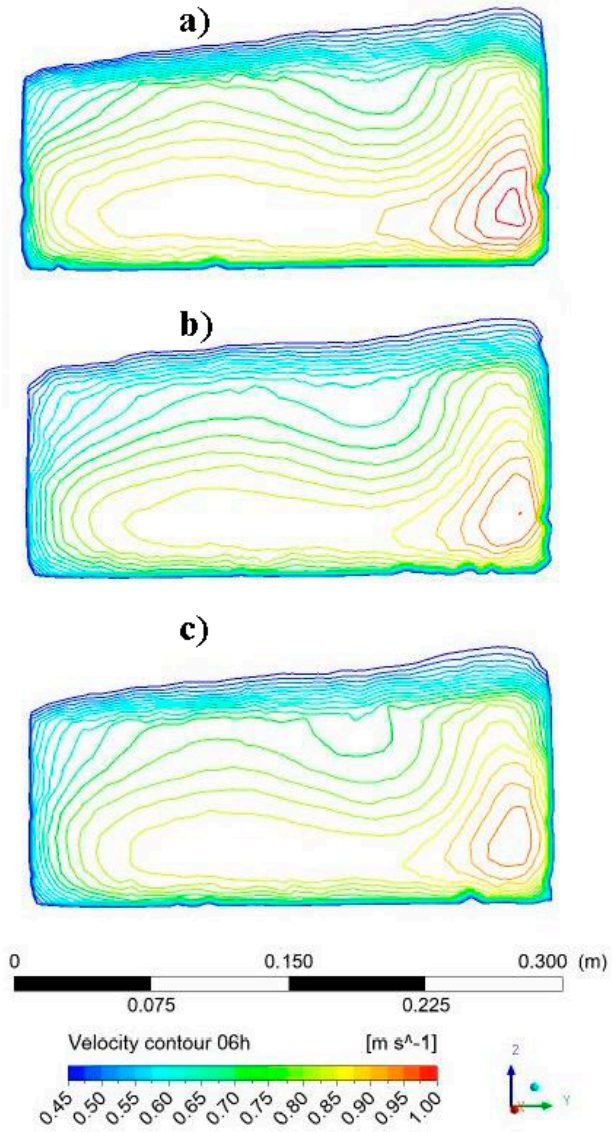

Figure 8. Velocity contours of "without vane" situation for Sections; (**a**) 1-1 (**b**) 2-2 (**c**) 3-3.

In the Figure 7 and Table 4, the flow velocity at sections was accepted as dimensionless velocity "u/u_{mean}". The 1st point represents the point close to the inner bank, and the 8th point represents the point close to the outer bank. The experimental and numerical model velocity values obtained in all sections are shown in Figure 7. Table 4 shows the error rates by comparing the experimental and CFD analysis results. In Figure 8a–c velocity contours of the 1-1, 2-2 and 3-3 cross-sections (without vane situation) are given, respectively.

When the table and graph are examined, it is seen that the error percentage of the velocities is less at the midpoints than at the edges. Maximum error was observed in the outer bank (8th points) for "without vane" situation 1-1 section (5–6%). In general, it has been found that the test and Fluent-CFD results are in good agreement. According to Figure 8a–c, it is seen that the velocity increases in the outer bank and decreases in the inner bank. In addition, as can be seen in the figure, the flow water depth decreases in the inner bank, while the water depth increases in the outer bank (the water depth changes with the blue contour lines). For the without vane situation, it is seen that the experiment and CFD results are generally compatible and the error rates are at a reasonable level.

The experimental and numerical model ("with vane") velocity values obtained in all sections are shown in Figure 9. Table 5 shows the error rates by comparing the experimental

and CFD analysis results in V_1 case. In Figure 10a–c velocity contours of the 1-1, 2-2 and 3-3 cross-sections ("with vane") are given, respectively.

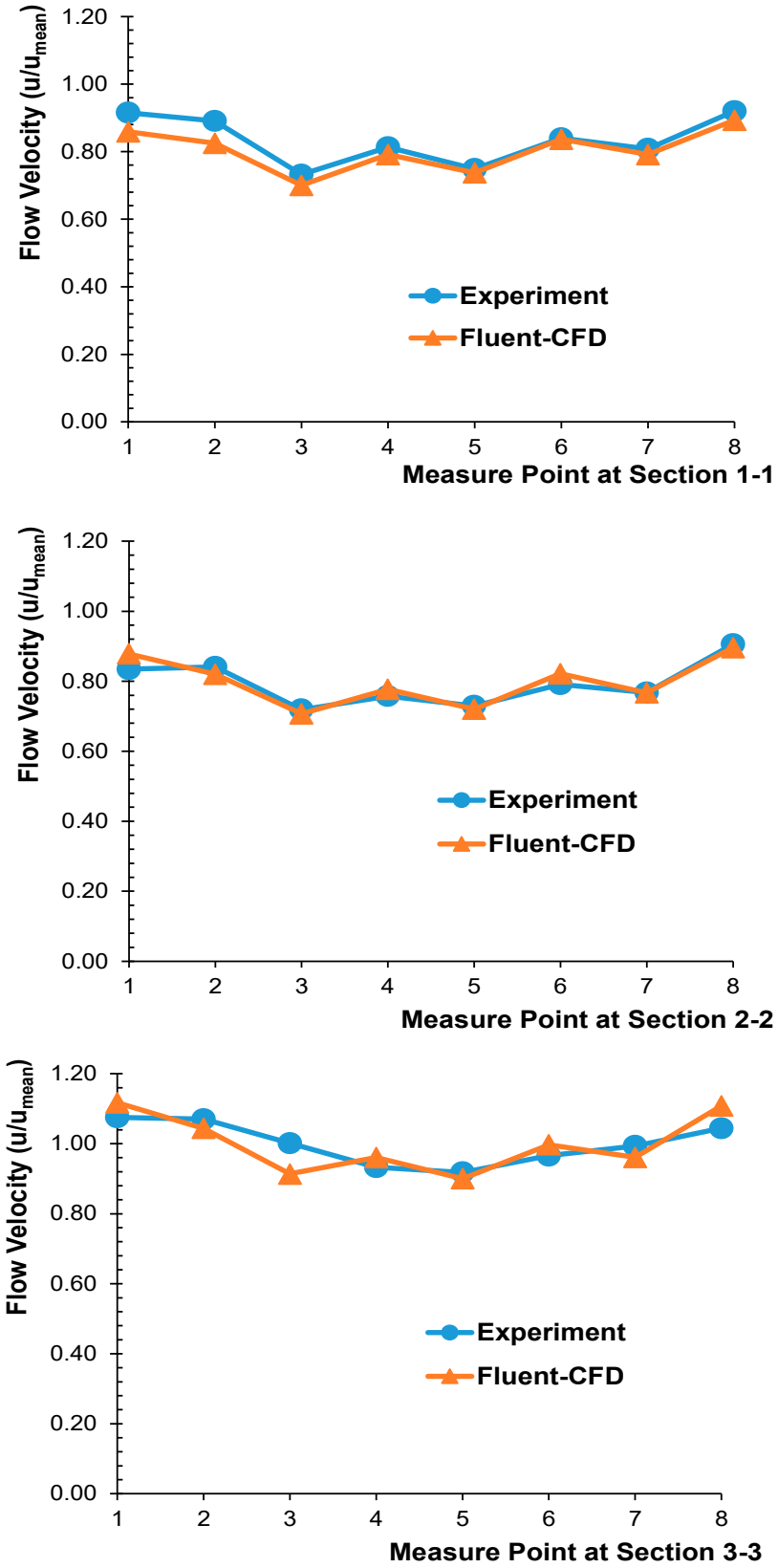

Figure 9. Flow velocity changes for 'with vanes' situation at sections; 1-1, 2-2 and 3-3.

Table 5. CFD and experimental velocity results for with vane situation at Sections 1-1, 2-2 and 3-3.

Section No	Point No	Location at x Direction (m)	Location at y Direction (m)	Experiment Results	Fluent CFD Results	Error (%)
1-1	1	1.10	0.247	1.10	1.07	2.81
	2	1.10	0.272	1.07	1.03	4.08
	3	1.10	0.297	0.88	0.87	0.83
	4	1.10	0.322	0.98	0.98	0.91
	5	1.10	0.347	0.90	0.92	2.08
	6	1.10	0.372	1.01	1.04	3.28
	7	1.10	0.397	0.97	0.98	1.46
	8	1.10	0.422	1.10	1.11	0.63
2-2	1	1.50	0.247	1.05	1.10	4.53
	2	1.50	0.272	1.06	1.03	3.10
	3	1.50	0.297	0.91	0.89	2.31
	4	1.50	0.322	0.95	0.97	1.96
	5	1.50	0.347	0.92	0.90	1.93
	6	1.50	0.372	1.00	1.03	3.17
	7	1.50	0.397	0.97	0.96	0.71
	8	1.50	0.422	1.14	1.12	1.70
3-3	1	1.70	0.247	1.08	1.10	2.35
	2	1.70	0.272	1.03	1.03	0.32
	3	1.70	0.297	0.99	0.93	6.32
	4	1.70	0.322	0.94	0.93	0.75
	5	1.70	0.347	0.93	0.93	0.37
	6	1.70	0.372	0.95	0.98	2.77
	7	1.70	0.397	1.03	1.00	3.48
	8	1.70	0.422	1.05	1.11	5.79

When the Table 5 was examined, maximum error was observed in 3-3 section (6.32%) for "with vane" situation. In general, it has been found that the test and Fluent-CFD results are in good agreement.

When the table and figures were examined, maximum error was observed in 3rd point) for "with vane" situation 3-3 section (6.32%). In general, it has been found that the experiment and Fluent-CFD results are in good agreement.

According to Figures 8 and 10, decreases in flow velocities are seen behind the vane. For the 1-1 section without the vane (Figures 8a and 10a), it was observed that the flow velocity decreased from 0,89 m/s to 0,70 m/s (3. point). It has been determined that there is a nearly 21% decrease in flow velocity. Compared to the 2-2 section without the vane (Figures 8b and 10b), it was observed that the flow velocity decreased from 0,93 m/s to 0.77 m/s (7. point). It has been determined that there is a nearly 18% decrease in flow velocity. Finally, the 3-3 section without the vane (Figures 8c and 10c), it was observed that the flow velocity decreased from 0,99 m/s to 0,72 m/s (5. point). It has been determined that there is a nearly 27% decrease in flow velocity. In addition to investigations of flow velocities, water levels for the V_0 and V_1 cases were also investigated. Water level changes given numerical contour with Vof in Figure 11 for V_0 and V_1 cases. In addition, CFD -water depth changes (as cm) in V_0 and V_1 case at for all sections.

When the depth changes in sections 1-1, 2-2 and 3-3 are examined (Figures 11 and 12), it is observed that generally submerged vanes increase the water depth. The most obvious change in section 1-1 (Figure 12a) was the increase in water height from 11 cm to 11.66 cm at the 5th point. It has been observed that it increases the water depth by about 6%. In section 2-2, it was observed that while the depth of flow increased slightly in the middle of the channel, the depth decreased at points 1 and 7 close to the outer and inner slope (Figure 12b). In the 3-3 section, it showed a similar change to the 1-1 section and the water level increased from 11 cm to 11.87 cm (Figure 12c). In the 3-3 section, the water depth increased by about 8% in the V_1 case compared to the V_0 case. When the changes in % are examined (Figure 12d), it can be said that there is a greater increase in the 1-1 and 3-3 sections than in the 2-2 sections.

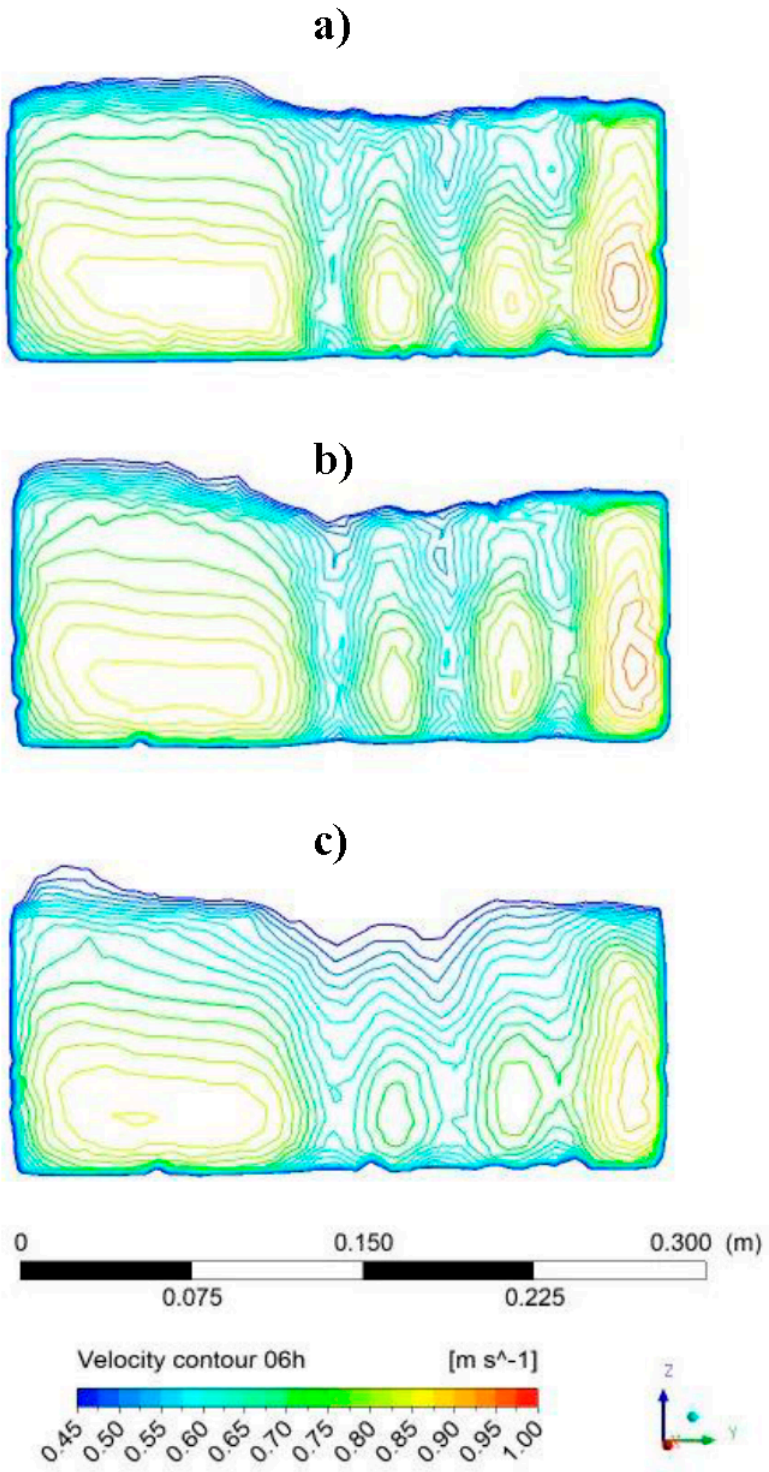

Figure 10. Velocity contours of 'with vanes' situation analysis (**a**) Section 1-1, (**b**) Section 2-2, (**c**) Section 3-3.

When all the velocity changes behind the submerged vane are examined (Figure 13), it is seen that the maximum velocity change (27%) is at the 3-3 section and at the 7. point, while the minimum change (16%) is at the 2-2 section and at the 5. point. For the velocity change between the vane, it is seen that the "maximum" velocity change (26%) is at the 3-3 section and at the 4. point, while the minimum change is at the 2-2 section and at the 6. Point (Figure 13).

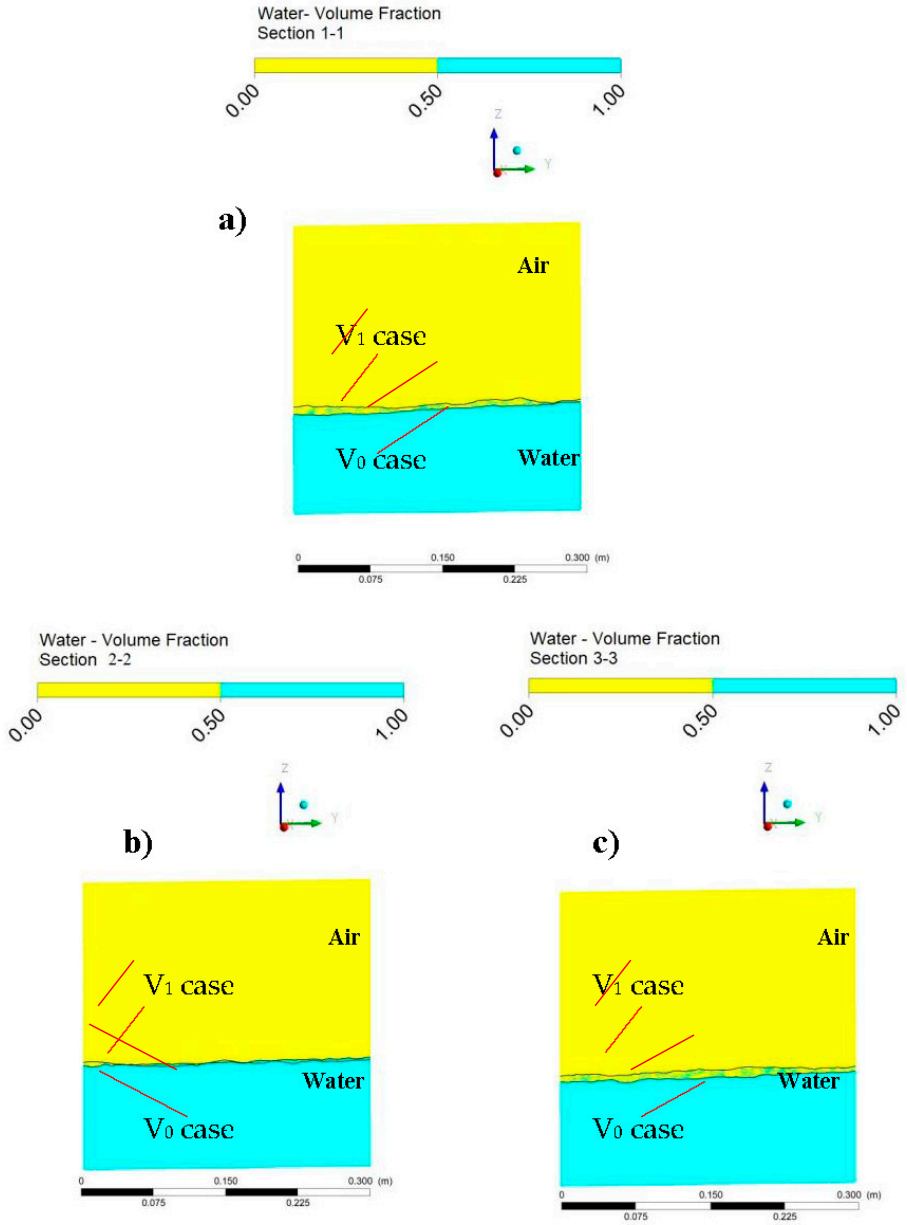

Figure 11. CFD -water level changes (m) in V_0 and V_1 case at (**a**) 1-1, (**b**) 2-2, (**c**) 3-3 sections.

In Figures 14 and 15, it was observed that while the mean velocities were approximately 0.75–0.83 m/s in the vaneless outer meander, these velocities decreased to an average of 0.61–0.68 m/s in the vaneless outer meander along the water depth. According to the after-vane structure's measurements, the submerged vanes reduced flow velocity by 21% in section 1-1, and decreased the flow velocity by 19% and 20% in sections 2-2 and 3-3, respectively.

Flow velocity profiles made without a submerged vane are compatible with numerical model or experiment results [19,30]. Reported laboratory experiments show flow patterns of submerged vanes. Scour in the outer meander was caused by the increase in flow velocity and shear stress. The submerged vane cuts off secondary circulation or cross flow cuts off thereby reducing high velocities around the outer meander (Figures 10, 11 and 15). This study investigated the effects of submerged vane structures on flow rates and water depth. As a result of this study, it was determined that submerged vane structures decrease the maximum and average velocity along the depth, decrease the flow velocity at 06 d and direct it to the inner bank. In the meander section of the open channel, velocity distribution diagrams of the submerged vaneless streamflow bed (Figures 7 and 8) show that it slides

out of the meander and reaches the maximum level near the outer meander before the outlet of the meander. This experimental pattern was consistent with experimental measurements in the other channel meander [19]. The centrifugal force increases proportionally with the square of the flow velocity and the upper region with high flow velocity reaches more centrifugal force than the lower region [30]. Experimental flow velocity results measured at 0.6 d, modeled both with submerged vane and without submerged vane, showed that the model with submerged vane decreased the flow velocity by 16–27% and directed the flow (Figures 7, 9 and 11). When the literature studies were examined, Gemici [7] experimentally found that submerged vane flow velocities were reduced by 7–19%. The flow models obtained with the 3D model were examined along with the depth (Figure 11), and it was observed that the mean velocity was reduced by 19–21% (Figures 14 and 15). The result of this study will be useful for understanding the flow phenomenon, validation of numerical work and subsequent design of meander protection measures.

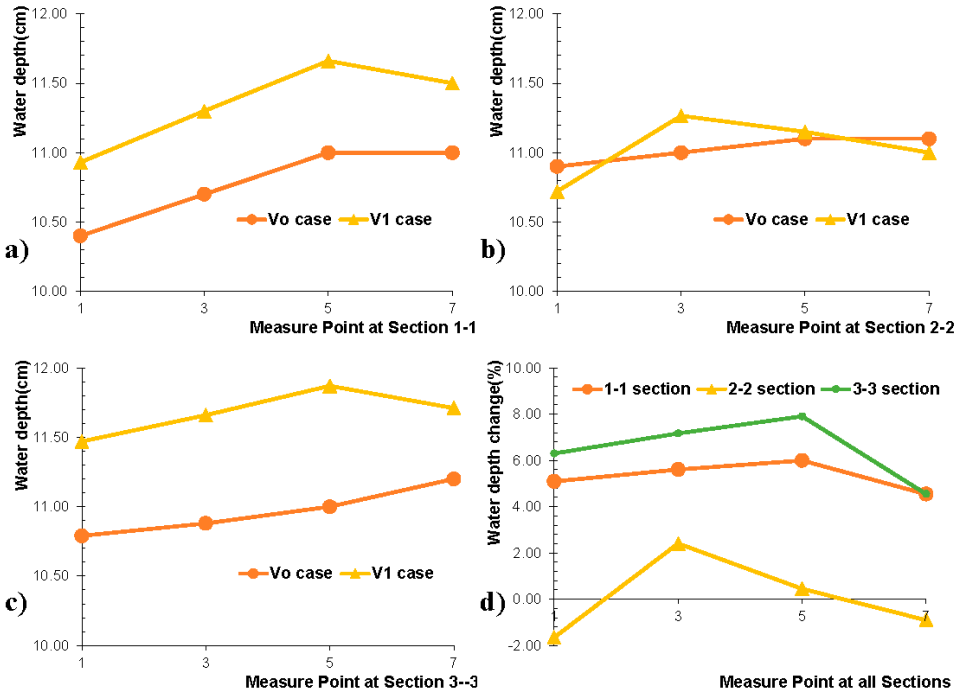

Figure 12. CFD -water depth changes (cm) in V_0 and V_1 case at (**a**) 1-1, (**b**) 2-2, (**c**) 3-3 sections and (**d**) % change for all sections.

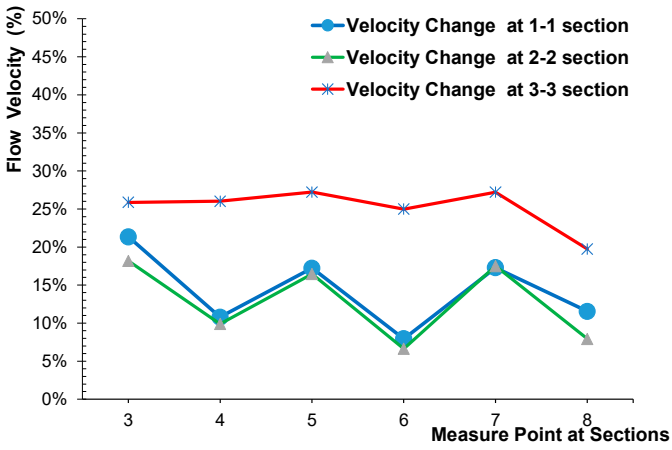

Figure 13. Flow velocity change according to 1-1, 2-2 and 3-3 sections for behind the submerged vane.

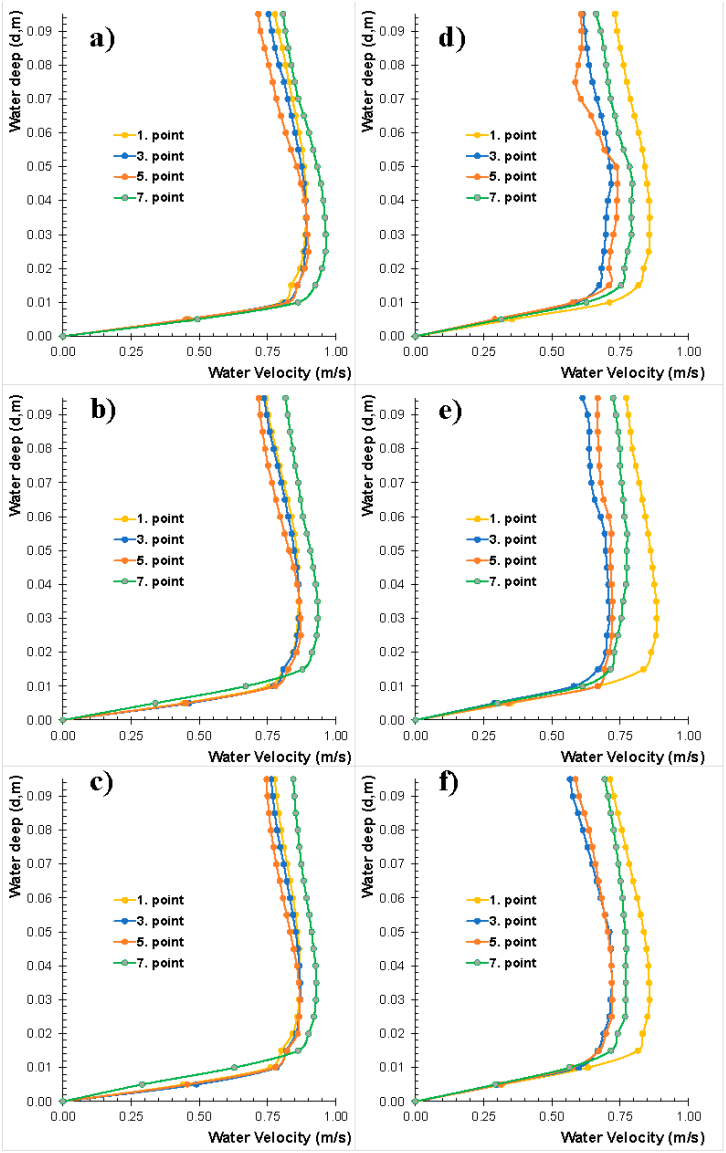

Figure 14. CFD -Velocity changes (m/s) along the water depth (m) in V_0 case points at (**a**) 1-1, (**b**) 2-2, (**c**) 3-3 sections and V_1 case points at (**d**) 1-1, (**e**) 2-2, (**f**) 3-3 sections.

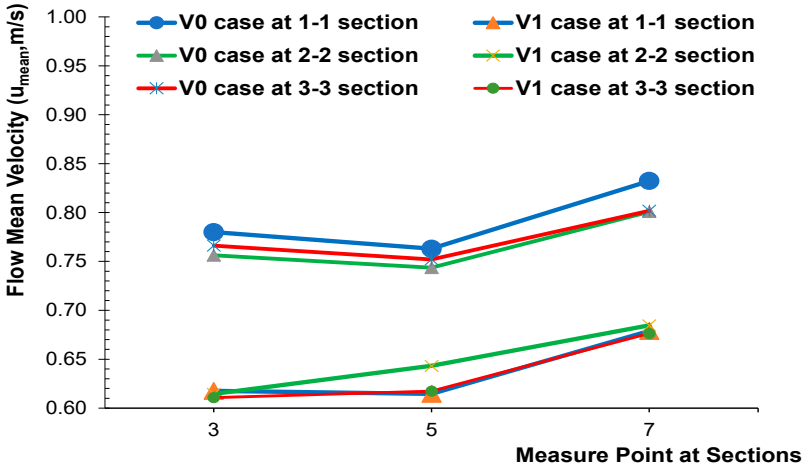

Figure 15. Flow velocity change according to the V_0 case and V_1 case.

4. Conclusions

In this study, the performance of without vane and 3-array vane models in open channel flows has been investigated by using a flow velocity of 25 L s^{-1}. The numerical results of the flow velocities were confirmed by experimental results. The effect of the vane structure on the flow velocity measured in the flow channel was determined and the 3 sectional velocity changes of the 3-array with 3 submerged vane ("with vane") structures were compared experimentally and numerically to each other. The following results can be derived from this study:

- The simulated CFD velocity for the without vane and 9 (3 × 3) vane cases were compared with the measured data. If the results of the experiments are examined in accordance with the CFD simulation results, a lower error has been detected. Figure 1. Flow velocity changes for 'with vanes' situation at sections; 1-1, 2-2 and 3-3. When the experimental and CFD results were examined, the maximum error was observed as 6.32%.
- It was found that 3 vane structures in 3-array affect the mean flow velocity by 27% and minimum flow velocity by 16% at 0.6 d.
- The flow velocities were investigated along with depth using the CFD and found that the mean velocity was reduced by 14–21% along the depth.
- Submerged vane structures balance the flow of water depth on the inner bank with the water depth on the outer bank within open channel flows. It reduced the flow velocity by directing the water depth and flow velocity from the outer bank to the inner bank.
- When the depth changes in sections are examined, it is observed that generally submerged vanes increase the water depth. In the sections, the water depth increased by about 6–8% in the V_1 case compared to the V_0 case.

Vane structures were found to be effective in regulating flow. It is also recommended that submerged vane structures be applied effectively in reducing flow velocities and directing strem flows.

Author Contributions: Conceptualization, M.Z. and F.Ü.; methodology, E.G.; software, B.T.; validation, F.Ü., M.Z. and E.G.; formal analysis, B.T.; investigation, B.T.; resources, E.G.; writing—original draft preparation, B.T.; writing—review and editing, F.Ü.; visualization, M.Z.; supervision, E.G.; project administration, F.Ü.; funding acquisition, M.Z. All authors have read and agreed to the published version of the manuscript.

Funding: This research received no external funding.

Data Availability Statement: Not applicable.

Acknowledgments: This work was supported by the Slovak Research and Development Agency under the Contract no. APVV-20-0281, This work was supported by project HUSKROUA/1901/8.1/0072 REVITAL.

Conflicts of Interest: The authors declare no conflict of interest.

References

1. Odgaard, A.J.; Kennedy, J.F. *Analysis of Sacramento River Bend Flows, and Development of a New Method for Bank Protection*; The University of Iowa: Iowa City, IA, USA, 1982. Available online: http://www2.iihr.uiowa.edu/wp-content/uploads/2013/06/IIHR241.pdf (accessed on 27 December 2022).
2. Odgaard, A.J.; Kennedy, J.F. River-Bend Bank Protection by Submerged Vanes. *J. Hydraul. Eng.* **1983**, *109*, 1161–1173. [CrossRef]
3. Odgaard, A.J.; Lee, H.Y.E. *Submerged Vanes for Flow Control and Bank Protection in Streams*; Iowa Institute of Hydraulic Research, the University of Iowa: Iowa City, IA, USA, 1984. Available online: https://agris.fao.org/agris-search/search.do?recordID=US874929288 (accessed on 27 December 2022).
4. Odgaard, A.J. Streambank Erosion along Two Rivers in Iowa. *Water Resour. Res.* **1987**, *23*, 1225–1236. [CrossRef]
5. Marelius, F.; Sinha, S.K. Experimental Investigation of Flow Past Submerged Vanes. *J. Hydraul. Eng.* **1998**, *124*, 542–545. [CrossRef]
6. Voisin, A.; Townsend, R.D. Model Testing of Submerged Vanes in Strongly Curved Narrow Channel Bends. *Can. J. Civ. Eng.* **2002**, *29*, 37–49. [CrossRef]
7. Gemici, E. *Açık Kanallarda Batık Kanatlarla Akım Yönetimi*; Erciyes Üniversity: Kayseri, Turkish, 2015.
8. Mohammadiun, S.; Salehi Neyshabouri, S.A.A.; Naser, G.; Vahabi, H. Numerical Investigation of Submerged Vane Effects on Flow Pattern in a 90° Junction of Straight and Bend Open Channels. *Iran. J. Sci. Technol. Trans. Civ. Eng.* **2016**, *40*, 349–365. [CrossRef]

9. Fathi, A.; Zomorodian, S.M.A. Effect of Submerged Vanes on Scour Around a Bridge Abutment. *KSCE J. Civ. Eng.* **2018**, *22*, 2281–2289. [CrossRef]
10. Kalathil, S.T.; Wuppukondur, A.; Balakrishnan, R.K.; Chandra, V. Control of Sediment Inflow into a Trapezoidal Intake Canal Using Submerged Vanes. *Port Coast. Ocean. Eng.* **2018**, *144*, 04018020. [CrossRef]
11. Zarei, E.; Vaghefi, M.; Hashemi, S.S. Bed Topography Variations in Bend by Simultaneous Installation of Submerged Vanes and Single Bridge Pier. *Arab. J. Geosci.* **2019**, *12*, 178. [CrossRef]
12. Lake, R.W.; Shaeri, S.; Senevirathna, S.T.M.L.D. Design of Submerged Vane Matrices to Accompany a River Intake in Australia. *J. Environ. Eng. Sci.* **2021**, *16*, 58–65. [CrossRef]
13. Gumgum, F.; Cardoso, A.H. Optimizing the Desilting Efficiency of Submerged Vane Fields at Lateral Diversions. *J. Hydraul. Eng.* **2022**, *149*, 04022031. [CrossRef]
14. Bor, A. Experimental Investigation of 90° Intake Flow Patterns with and without Submerged Vanes under Sediment Feeding Conditions. *Can. J. Civ. Eng.* **2021**, *49*, 452–463. [CrossRef]
15. Üneş, F. Investigation of Density Flow in Dam Reservoirs Using a Three-Dimensional Mathematical Model Including Coriolis Effect. *Comput. Fluids* **2008**, *37*, 1170–1192. [CrossRef]
16. Ünes, F. Prediction of Density Flow Plunging Depth in Dam Reservoirs: An Artificial Neural Network Approach. *Clean* **2010**, *38*, 296–308. [CrossRef]
17. Üneş, F.; Demirci, M.; Varçin, H. 3-D Numerical Simulation of a Real Dam Reservoir: Thermal Stratified Flow. *Springer Water* **2016**, 377–394. [CrossRef]
18. Üneş, F.; Varçin, H. Investigation of Seasonal Thermal Flow in a Real Dam Reservoir Using 3-D Numerical Modeling. *J. Hydrol. Hydromech.* **2015**, *63*, 38–46. [CrossRef]
19. Odgaard, A.J. River Training and Sediment Management with Submerged Vanes. *River Train. Sediment Manag. Submerg. Vanes* **2009**. [CrossRef]
20. Turhan, E.; Ozmen-Cagatay, H.; Kocaman, S. Experimental and Numerical Investigation of Shock Wave Propagation Due to Dam-Break Over a Wet Channel. *Pol. J. Environ. Stud.* **2019**, *28*, 2877–2898. [CrossRef]
21. Ozmen-Cagatay, H.; Turhan, E.; Kocaman, S. An Experimental Investigation of Dam-Break Induced Flood Waves for Different Density Fluids. *Ocean Eng.* **2022**, *243*, 110227. [CrossRef]
22. Launder, B.E.; Spalding, D.B. *Mathematical Models of Turbulence*; Academic Press: New York, NY, USA, 1972.
23. Kim, H.; Nanjundan, P.; Lee, Y.W. Numerical Study on the Sloshing Flows in a Prismatic Tank Using Natural Frequency of the Prismatic Shapes. *Prog. Comput. Fluid Dyn.* **2021**, *21*, 152–160. [CrossRef]
24. Simsek, O.; Akoz, M.S.; Soydan, N.G. Numerical Validation of Open Channel Flow over a Curvilinear Broad-Crested Weir. *Prog. Comput. Fluid Dyn.* **2016**, *16*, 364–378. [CrossRef]
25. Hirt, C.W.; Nichols, B.D. Volume of Fluid (VOF) Method for the Dynamics of Free Boundaries. *J. Comput. Phys.* **1981**, *39*, 201–225. [CrossRef]
26. ANSYS Analysis Systems Fluid Simulation Software. Available online: https://www.ansys.com/products/fluids (accessed on 27 December 2022).
27. Salim, S.M.; Ariff, M.; Cheah, S.C. Wall Y+ Approach for Dealing with Turbulent Flows over a Wall Mounted Cube. *Prog. Comput. Fluid Dyn.* **2010**, *10*, 341–351. [CrossRef]
28. Gerasimov, A. Modeling Turbulent Flows with Fluent. Available online: http://www.ae.metu.edu.tr/seminar/Turbulence_Seminar/Modelling_turbulent_flows_with_FLUENT.pdf (accessed on 27 December 2022).
29. Unes, F.; Varcin, H. 3-D Real Dam Reservoir Model for Seasonal Thermal Density Flow. *Environ. Eng. Manag. J.* **2017**, *16*, 2009–2024. [CrossRef]
30. Biswas, P.; Barbhuiya, A.K. Effect of Submerged Vane on Three Dimensional Flow Dynamics and Bed Morphology in River Bend. *River Res. Appl.* **2019**, *35*, 301–312. [CrossRef]